Supplementary Information (SI) for Inorganic Chemistry Frontiers.
This journal is © the Partner Organisations 2026

Supporting Information

Comparative insights into the role of oxygen vacancies in α-MnO_2 for activating peroxymonosulfate and peroxydisulfate

Qianwei Li [a#], *Daoqing Liu** [a#], *Wei Yan* [a], *Hao Liu* [a], *Chunmao Chen* [a]

[a] State Key Laboratory of Heavy Oil Processing, China University of Petroleum, Beijing 102249, China

[#] Both authors contributed equally to this work.

*To whom correspondence should be addressed:

liudaoqing@cup.edu.cn (D.Q.Liu)

Supplementary Text, Figures, and Tables

Text S1. Batch experiment

All solutions used in the experiments were prepared with deionized water. The reactions were carried out at room temperature with magnetic stirring at 600 rpm in a beaker. Before the reaction started, the catalyst (400 mg/L) was added to 50 mL of Acid Orange II (AO II) solution (0.1 mM) to ensure thorough dispersion. Then, 4 mM PDS or 0.13 mM PMS was added to initiate the reaction. At predetermined intervals, samples were taken and immediately filtered through a 0.45 μm membrane. Subsequently, 0.5 mL of the filtrate was accurately mixed with 0.5 mL of methanol (MeOH) to quench the degradation reaction. The initial pH of the reaction solution was adjusted using 1 mol/L H_2SO_4 and 1 mol/L NaOH solutions.

Before concentration measurements, a standard calibration curve was established to ensure sample concentrations fell within the linear range. The concentration of AO II was determined by UV–Visible spectrophotometry (Thermo Scientific Nicolet 6700, USA). First, a 1 g/L AO II stock solution was diluted into a series of standard solutions with different concentrations. The absorbance of these standards was measured at the maximum absorption wavelength of 484 nm. A calibration curve was plotted with AO II concentration on the x-axis and absorbance (A) on the y-axis, yielding a linear regression equation. During measurements, the background absorbance of the blank electrolyte was subtracted from all absorbance data to calculate the corresponding AO II concentration. Each experiment was repeated at least three times, and the average values were reported.

This study employed two spin-trapping agents: 5,5-dimethyl-1-pyrroline N-oxide (DMPO, >99%, Sigma-Aldrich) and 2,2,6,6-tetramethyl-4-piperidinol (TEMP, >99%, Sigma-Aldrich), to capture radicals and singlet oxygen generated during the reactions. Specifically, DMPO and TEMP were separately dissolved in phosphate buffer solution at pH 7.4, with final concentrations of 80 mM and 50 mM, respectively. Then, 1 mL of sample was taken from the α-MnO_2/PDS reaction system (containing 40 mM DMPO or 25 mM TEMP, catalyst at 400 mg/L, PDS at 4 mM or FFA at 100 μM), and filtered through a 0.45 μm membrane. Finally, a small amount of the resulting mixture was drawn into a quartz capillary tube and subjected to EPR analysis to detect the spin-trapped adducts.

Text S2. Electrochemical Analysis

(1) Preparation of carbon-coated glassy carbon electrode

A catalyst-coated glassy carbon electrode was prepared by dipping a glassy carbon electrode (GCE) into a solution. Before the dipping process, the glassy carbon electrode was polished with alumina powder. To obtain a homogeneous ink, 5 mg of the α-MnO_2 material was dispersed in 1 mL of a Nafion-containing solution (comprising 150 μL of isopropanol, 800 μL of ultrapure water, and 500 μL of a 5 wt.% Nafion solution) under ultrasonication for 1 h. A working electrode was prepared by dipping 8 μL of the catalyst into a glassy carbon electrode (5 mm in diameter) and drying at ambient temperature (25°C) for 6 hours. The working electrode was activated by cyclic voltammetry (CV) cycling between 0 and 1.0 V (*vs.* RHE) at a scan rate of 10 mV s^{-1} in 0.1 M Na_2SO_4 solution to obtain a stable voltammogram.

(2) Analytical methods for electrochemically active specific surface area (ECSA)

The ECSA was estimated by measuring the capacitive current associated with double-layer charging from the scan-rate dependence of cyclic voltammograms (CVs). All ECSA tests were conducted in a 0.1 M Na_2SO_4 electrolyte using a three-electrode cell with a Pt plate serving as the counter electrode, Ag/AgCl as the reference electrode, and the as-prepared catalyst-modified electrode as the working electrode. The potential window of CVs was 0.6–0.7 V *vs.* RHE, and the scan rates were 20, 40, 60, 80, and 100 mV s^{-1}. The double-layer capacitances (C_{dl}) of various samples were determined from the CVs, which are expected to be linearly proportional to the effective surface area. The double-layer capacitance was estimated by plotting the $\Delta J = J_a - J_c$ (i.e., the difference of the anode current density J_a and cathode current density J_c) at 0.65 V *vs.* SCE against the scan rate. The linear slope is equivalent to twice the double-layer capacitance Cdl, which can be used to represent the electrochemical active surface area [1].

(2) Potential conversion

The measured potentials can be converted to the corresponding potentials of the reversible hydrogen electrode through the formula $E_{RHE}=E_{SCE}+0.242+0.0591*pH$.

Text S3. DFT Method

All density functional theory (DFT) calculations were carried out using the Vienna *Ab initio* Simulation Package (VASP) [2, 3]. The exchange–correlation effects were treated with the generalized gradient approximation (GGA) in the Perdew-Burke-Ernzerhof (PBE) formalism [4]. The interaction between core and valence electrons was described by the projector augmented wave (PAW) method [5]. A plane-wave cutoff energy of 400 eV was employed for all calculations, and the Brillouin zone was sampled using a 3×2×1 Monkhorst-Pack *k*-point mesh. The electronic self-consistency and ionic relaxation were converged to 1.0×10^{-5} eV in total energy and 0.05 eV $Å^{-1}$ in residual forces, respectively. Long-range van der Waals interactions were included using the DFT-D3 dispersion correction scheme [6]. Structural models and charge/geometry analyses were visualized using the VESTA software package [7].

The adsorption energy (E_ad_s) of species A on the catalyst surface was evaluated as:

$$E_{ads} = E_{A*} - E_A - E_{sub}$$

where E_{A*} is the total energy of the adsorbed system, E_A is the energy of the isolated A molecule, and E_{sub} is the energy of the clean substrate.

HRTEM images of ultrasound-treated α-MnO_2

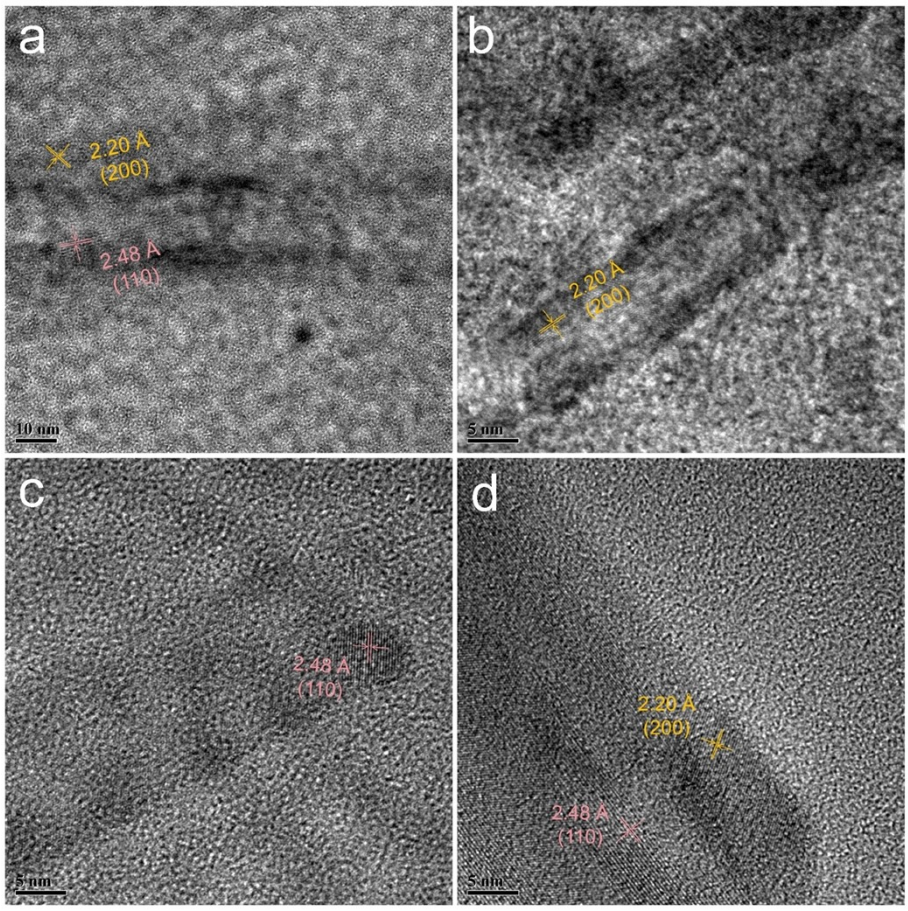

Fig. S1. HRTEM images and (a–d) of α-MnO_2, α-MnO_2-OV-0.5, α-MnO_2-OV-1, and α-MnO_2-OV-3.

Summary of XPS data for ultrasound-treated α-MnO_2

Table S1. XPS data for ultrasound-treated α-MnO_2 with different conditions.

Sample	Mn (%)				O (%)			AOS
	Mn^{2+}	Mn^{3+}	Mn^{4+}	Mn^{3+}/Mn^{4+}	O_{latt}	O_{ads}	O_{latt}/ O_{ads}	(Mn)
α-MnO_2	6.49	39.86	53.66	0.743	66.96	26.88	2.49	3.62
α-MnO_2-OV-0.5	4.32	51.24	44.44	1.15	60.51	31.75	1.91	3.54
α-MnO_2-OV-1	3.52	55.38	41.10	1.35	55.58	36.5	1.52	3.52
α-MnO_2-OV-3	3.77	59.55	36.68	1.62	48.32	33.46	1.44	3.48

Adsorption of AO II by the α-MnO_2

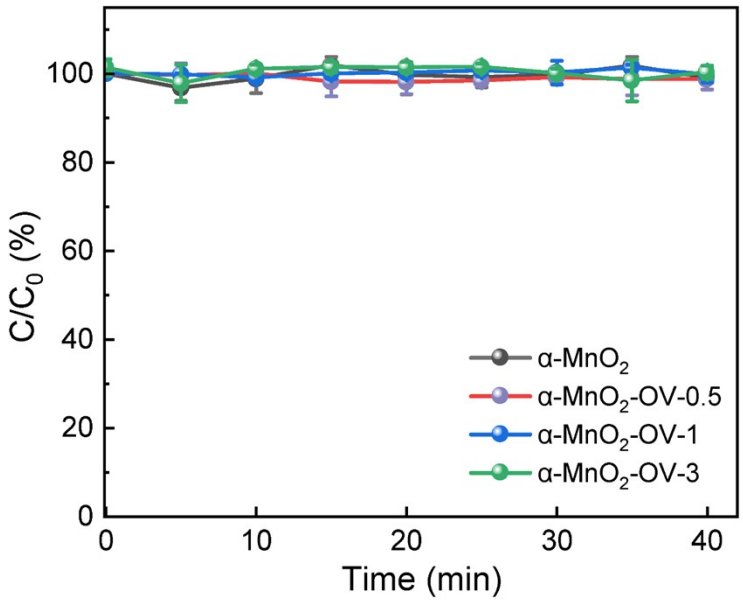

Fig. S2. Adsorption of performance AO II by α-MnO_2, α-MnO_2-OV-0.5, α-MnO_2-OV-1, and α-MnO_2-OV-3.

Degradation of AO II by the α-MnO_2/PMS system with radical scavengers

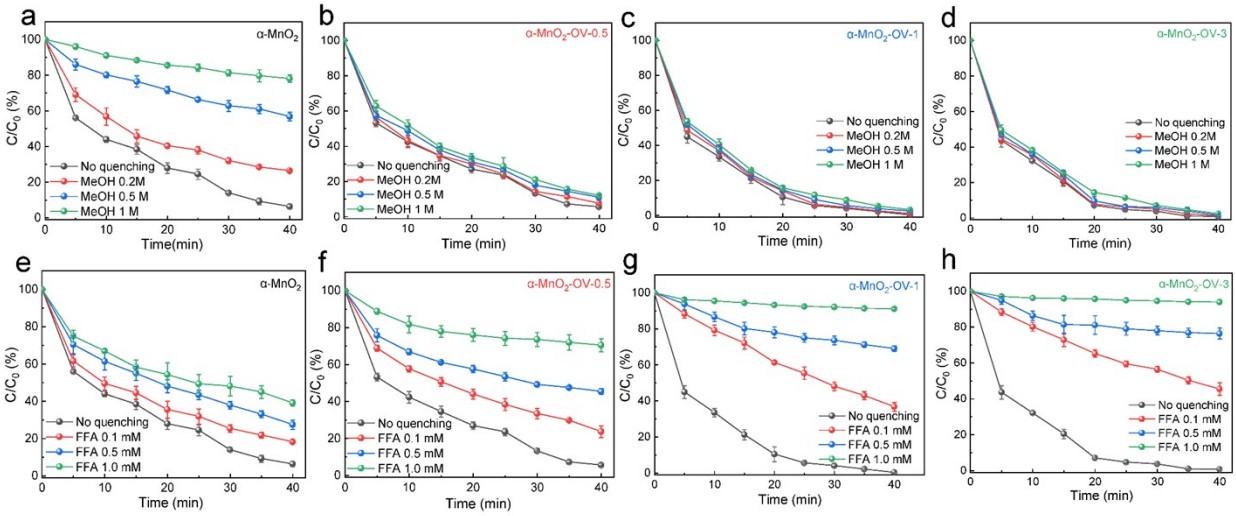

Fig. S3. Degradation of AO II by the α-MnO_2/PMS system in the presence of methanol (a–d) and FFA (e–h) as radical scavengers. ([AO II]$_0$ = 0.1 mM, [Material] = 400 mg/L, [PMS] = 0.13 mM, pH≈7.0)

Effect of ultrasound on ECSA of α-MnO_2

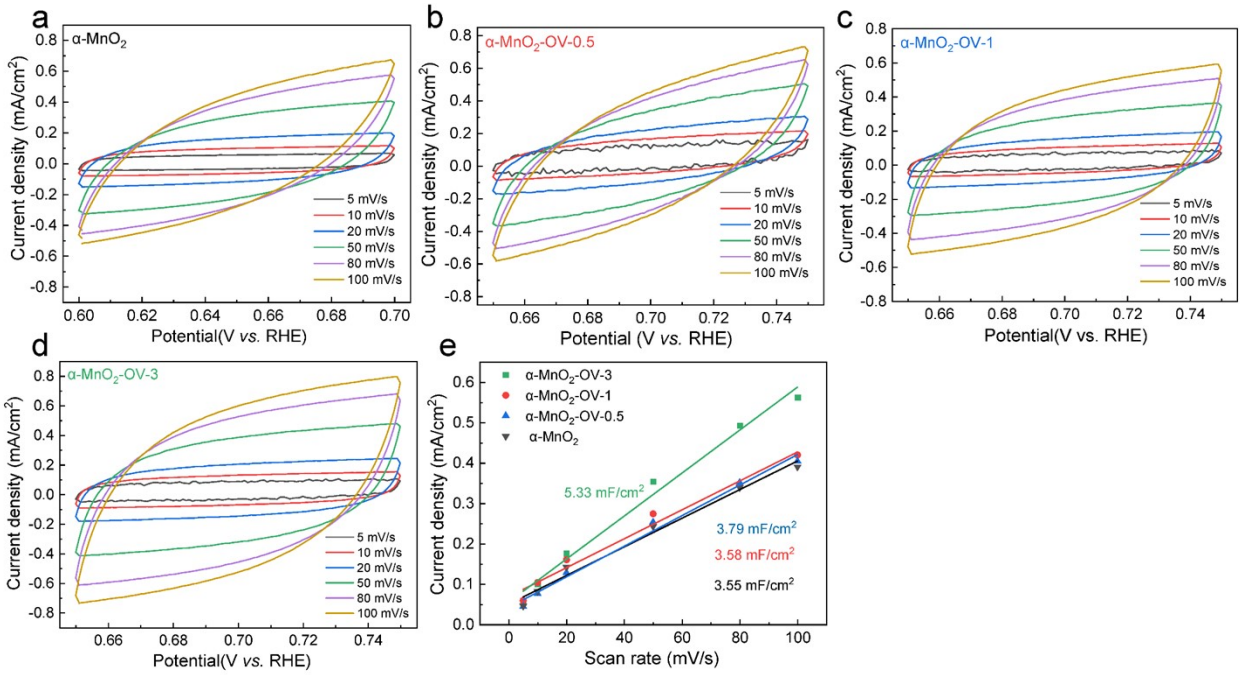

Fig. S4. CV curves of (a) α-MnO_2 (b) α-MnO_2-OV-0.5, (c) α-MnO_2-OV-1, (d) α-MnO_2-OV-3, at different scan rates, and (e) ECSA measurements of samples based on the double-layer capacitance over a range of scan rates.

Effect of aeration on PMS activation by α-MnO_2-OV-1

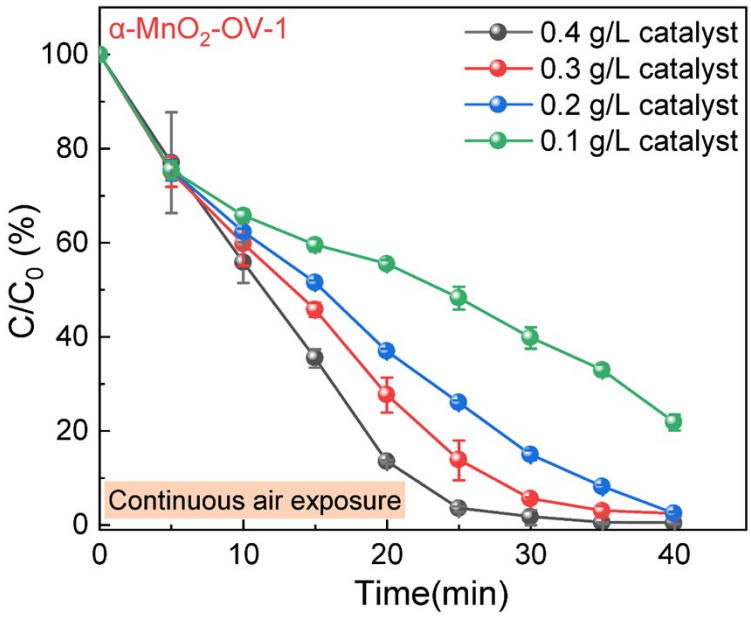

Fig. S5. Degradation performance of α-MnO_2-OV-1under continuous air exposure conditions (air flow rate: 200 mL/min, $[AO\ II]_0$ = 0.1 mM, [Material] = 400 mg/L, [PMS] = 0.13 mM, pH≈7.0)

XPS spectra of the α-MnO_2-OV-1 after being used for PMS activation

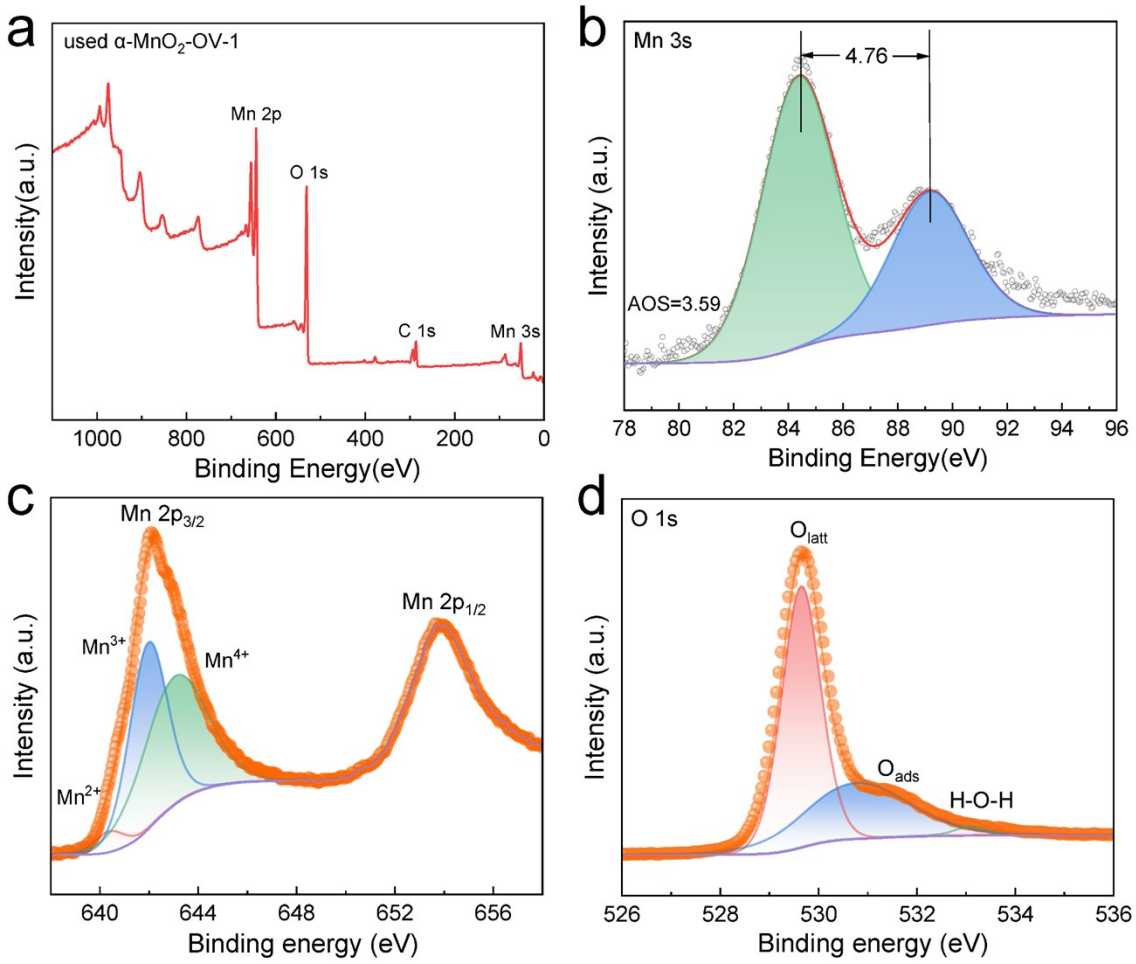

Fig. S6. XPS spectra for survey spectra (a), Mn 3s (b), Mn $2p_{3/2}$ (c), O 1s (d), of the α-MnO_2-OV-1 after being used for PMS activation.

Table S2. XPS data for ultrasound-treated α-MnO_2-OV-1 after being used for PMS activation.

Sample	Mn (%)				O (%)			AOS (Mn)
	Mn^{2+}	Mn^{3+}	Mn^{4+}	Mn^{3+}/Mn^{4+}	O_{latt}	O_{ads}	O_{latt}/O_{ads}	
Used α-MnO_2-OV-1	3.68	44.45	51.86	0.857	62.73	35.68	1.75	3.59

DFT calculation of PDS and PMS adsorption on the MnO_2 (200)

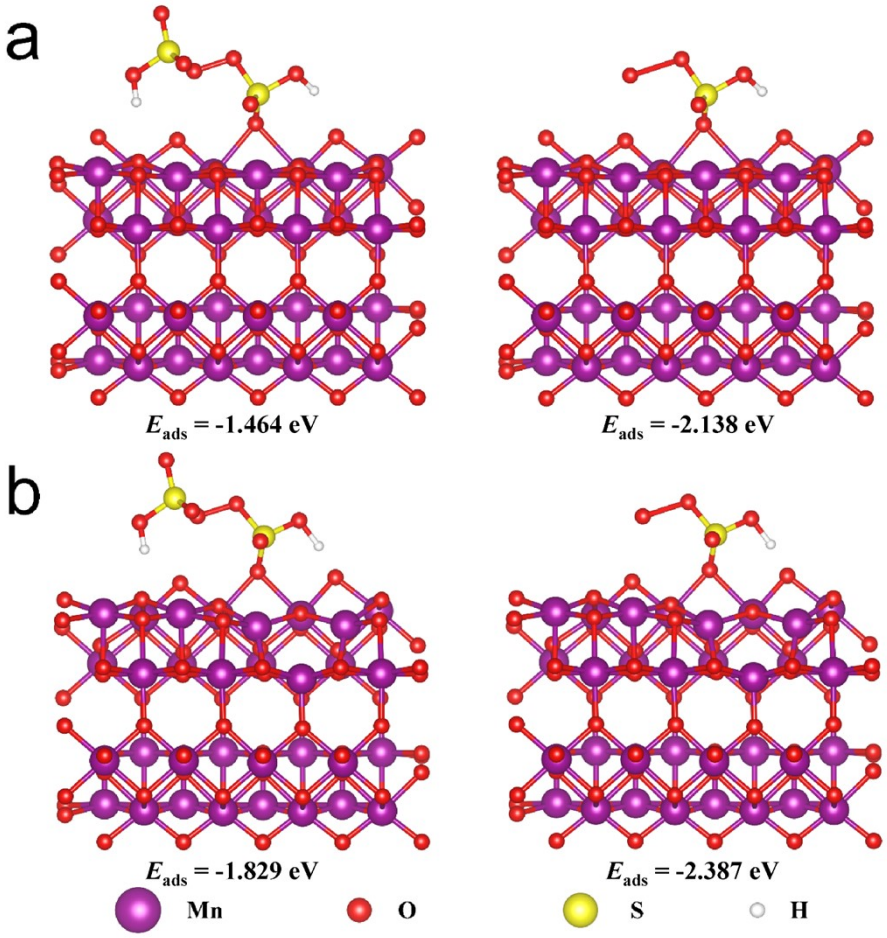

Fig. S7. DFT calculation of PDS or PMS adsorption on the MnO_2 (200) with (a) one and (b) three oxygen vacancies.

Reference

1. D. Liu, Y. Zhou, B. Wei, Q. Li and H. Zhao, Analyzing the active sites of carbocatalyst for peroxydisulfate activation: Specific surface area or electrochemical surface area?, *Chemosphere*, 2024, **364**, 143124.
2. G. Kresse and J. Hafner, Ab initio molecular dynamics for open-shell transition metals, *Phys Rev B*, 1993, **48**, 13115-13118.
3. G. Kresse and J. Furthmüller, Efficient iterative schemes for ab initio total-energy calculations using a plane-wave basis set, *Phys Rev B*, 1996, **54**, 11169-11186.
4. J. P. Perdew, K. Burke and M. Ernzerhof, Generalized Gradient Approximation Made Simple, *Phys Rev Lett*, 1996, **77**, 3865-3868.
5. G. Kresse and D. Joubert, From ultrasoft pseudopotentials to the projector augmented-wave method, *Phys Rev B*, 1999, **59**, 1758-1775.
6. S. Grimme, J. Antony, S. Ehrlich and H. Krieg, A consistent and accurate ab initio parametrization of density functional dispersion correction (DFT-D) for the 94 elements H-Pu, *J. Chem. Phys.*, 2010, **132**.
7. K. Momma and F. Izumi, VESTA 3 for three-dimensional visualization of crystal, volumetric and morphology data, *J Appl Crystallogr*, 2011, **44**, 1272-1276.